Thermal characterization of surface acoustic wave devices

C. Huck, H. P. Zidek, T. Ebner, K. C. Wagner, Achim Wixforth

Angaben zur Veröffentlichung / Publication details:

Huck, C., H. P. Zidek, T. Ebner, K. C. Wagner, and Achim Wixforth. 2013. "Thermal characterization of surface acoustic wave devices." In *2013 IEEE International Ultrasonics Symposium (IUS), 21-25 July 2013, Prague, Czech Republic*, 1089–92. Piscataway, NJ: IEEE. https://doi.org/10.1109/ultsym.2013.0279.

10.1109/ULTSYM.2013.0279

Thermal Characterization of Surface Acoustic Wave Devices

C. Huck[1,2], H. P. Zidek[2], T. Ebner[2], K. C. Wagner[2], and A. Wixforth[1]

[1] Institute of Physics, University of Augsburg, 86159 Augsburg, Germany
[2] TDK Corporation, 81671 Munich, Germany
Email: christian.huck@physik.uni-augsburg.de

***Abstract*—Reliability of micro-electronic devices is one of the most important issues in mobile communication systems and is significantly influenced by the thermal behavior of the components. This study presents different schemes for thermal characterization of a half-section ladder-type Surface Acoustic Wave (SAW) filter which is acoustically passivated with a thick SiO_2 layer. Unitarity violation quantifies the entire power loss in the device but is unfeasible regarding correlation to each resonator. The Temperature Coefficient of Frequency (TCF) characterizes thermally induced frequency shifts and has the potential to investigate the resonators' temperatures separately in first order. However, uncertainties arise using this indirect approach as soon as other effects causing a frequency shift play a role. Thermographic techniques such as Infrared Thermography (IRT) and Liquid Crystal Thermography (LCT) serve as direct measurement schemes eliminating inaccuracies inherent to TCF based evaluations and show good agreement with simulation results. Moreover, LCT and IRT provide spatially resolved temperature measurements of the component.**

I. Introduction

Modern mobile communication systems impose high demands on Radio-Frequency (RF) filtering applications. Devices based on Surface Acoustic Wave (SAW) technology meet these requirements very well. However, despite many years of research and development, domains such as reliability and lifetime are still subject of current investigations [1]. They need to be thoroughly studied especially since mobile applications require continuous reduction in component size. One of the important issues deteriorating the device reliability is the increase of internal temperature due to power dissipation in the component. This self-heating causes crucial frequency shifts of the filter characteristics at high electrical power levels as well. Therefore, investigating the temperature behavior of SAW resonators is an important task regarding reliability and is also necessary to optimize the filter design.

II. Thermal Characterization

In this study, we present different schemes for characterization of the thermal behavior of acoustically passivated SAW devices. This includes electrical approaches like unitarity violation and evaluation of temperature induced frequency shifts as well as optical approaches by thermographic techniques.

A. Unitarity Violation

In general, temperature increase in every electronic device is mainly induced by loss mechanisms which transform electrical or mechanical energy into thermal energy. In this way, investigating losses in the device gives information about its thermal behavior indirectly. The following considerations are based on simulations because they allow for a detailed inspection of fundamental physical quantities.

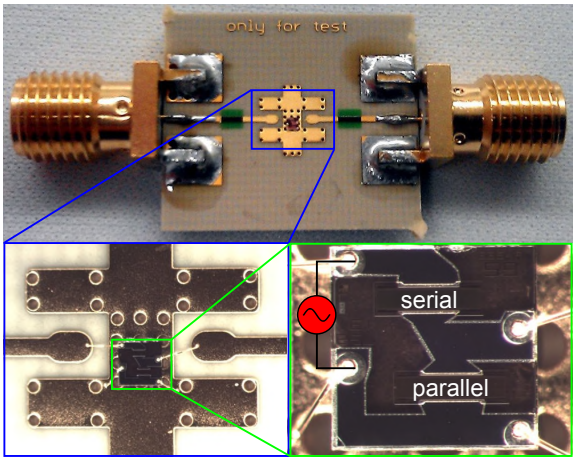

Fig. 1. The investigated device is a half-section ladder-type SAW filter consisting of one serial and one parallel resonator with the former next to the input. It is acoustically passivated with a 5 µm thick SiO_2 layer and mounted on a PCB by an epoxy adhesive.

This study focuses on a half-section ladder-type filter consisting of one serial and one parallel resonator (Fig. 1). Since this circuitry represents the constitutive element of each RF duplexer it contains ample information for subsequent filter designs. The pitches of both resonators in this structure are designed such that the parallel resonator has its resonance at the left filter skirt and the serial resonator has its antiresonance at the right filter skirt which is visualized in the logarithmic admittance plot of Fig. 2(a). Consequently, the parallel resonator's antiresonance and the serial resonator's resonance are located within the passband.

Fig. 2(b) and Fig. 2(c) show the corresponding absolute values of currents and voltages, respectively. At the left filter skirt, the parallel resonator is in resonance corresponding to minimum impedance and resulting in maximum current and minimum voltage drop. Since the serial resonator is located in front of the parallel one, both current values converge and due to its larger impedance compared to the parallel resonator the voltage drop in the serial one is bigger. At the right filter skirt, the serial resonator is in antiresonance denoting maximum impedance and resulting in minimum current and maximum voltage drop. The current and voltage drop of the parallel resonator is negligible because it is located after the serial

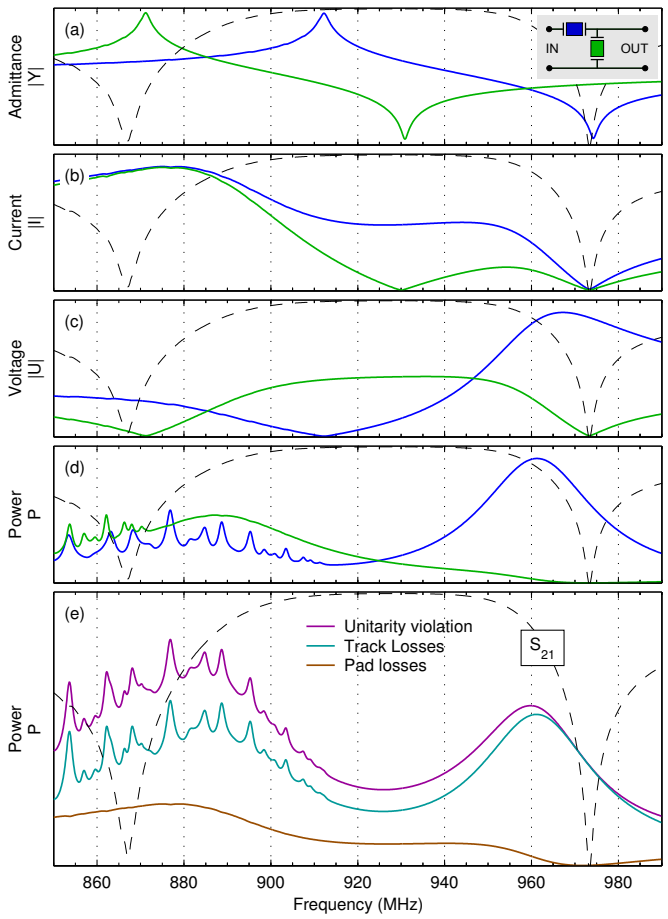

Fig. 2. Simulation of a half-section ladder-type SAW filter: (a) Admittances, (b) currents, (c) voltages, and (d) track losses of the serial (blue) and parallel (green) resonator as sketched in the inset by the equivalent circuit. The bottom panel (e) shows the unitarity violation, the total track losses in both resonators, and the difference of these two values quantifying all losses outside the tracks. As a reference, the transfer function S_{21} of the filter is added in all plots in arbitrary units.

one. Within the passband, similar considerations clarify that the minimum current flow of the parallel resonator occurs at its antiresonance and the minimum voltage drop of the serial resonator at its resonance.

The dissipated power in each resonator shown in Fig. 2(d) can be determined approximately by evaluating $P = \mathrm{Re}(\mathbf{U}^\dagger \mathbf{I})$ with the superscript $[\,]^\dagger = [^*]^T$ representing the transpose conjugation. So far, we only investigated each resonator's interdigital transducer but a detailed analysis requires consideration of interactions between all ports including the reflectors. This is satisfied by calculating $P = \mathrm{Re}(\mathbf{U}^\dagger \mathbf{Y} \mathbf{U})$ using the entire admittance matrix. Summing up the dissipated power in both resonators yields the combined dissipated power in both tracks referred to as track losses in Fig. 2(e). The noticeable distortions below the resonance frequency of each resonator are caused by Fabry-Pérot interferences due to finite dimensions of the resonators.

Because measurements reveal only scattering parameters, we discuss the applicability of these physical quantities for characterization of loss mechanisms in the following. Due to energy conservation reasons, in a lossless network the scattering matrix $\mathbf{S}$ has to be unitary

$$\mathbf{S}^\dagger \mathbf{S} = \mathbf{I} \,,$$

where $\mathbf{I}$ denotes the unity matrix. For a two-port lossy network, the unitarity condition simplifies and due to arising losses transforms into an inequation

$$|S_{11}|^2 + |S_{21}|^2 < 1 \,,$$

which is referred to as unitarity violation. In Fig. 2(e) the simulated unitarity violation is contrasted with the total track losses in both resonators. Since the unitarity violation quantifies the entire power loss in the device, the deviation to the track losses results in the overall power loss outside the active tracks referred to as pad losses. Those are originated in the pads, bond wires, and the PCB and therefore correlate with the respective current. Variations due to Fabry-Pérot interferences do almost not appear in the pad losses because they are only influencing the track losses which are also inherently included in the unitarity violation.

The simulation results demonstrate that with knowledge of pad losses the combined power loss in both tracks can be identified and related to each resonator by considering the ratios from Fig. 2(d). However, in measurement it is impossible to detect the pad losses and, thus, unitarity violation only indicates globally arising losses in the device precluding localization to each resonator.

B. Temperature Coefficient of Frequency

The thermal frequency stability of resonators is characterized by the Temperature Coefficient of Frequency (TCF). It is defined as the relative change in frequency with temperature

$$\mathrm{TCF} = \frac{1}{f}\frac{df}{dT} \,,$$

and is usually expressed in ppm/K. Because duplexers are required to operate within a prescribed frequency band over wide temperature ranges, reducing TCF is very important and big efforts are made to realize even zero TCF devices [2]. Vice versa, in devices with non-zero TCF the frequency shift of the transfer function can be used to determine the component's temperature increase indirectly.

In this method, the transfer function of the unloaded filter is measured for different ambient temperatures. Evaluating the frequency shift at a predefined attenuation level results in the TCF for the left and the right filter skirt (Fig. 3). Subsequently, these values serve as quantities to map the frequency shift of the loaded filter to the temperature increase. Defining the attenuation level relatively to the minimum insertion loss instead of using absolute levels avoids falsification of the results due to modification of the filter characteristics under thermal or electrical loading. Since the left filter skirt is mainly dominated by the parallel resonator and the right skirt by the serial resonator (Fig. 2), with this method the self-heating of each resonator can be determined separately with the presumption of negligible thermal coupling.

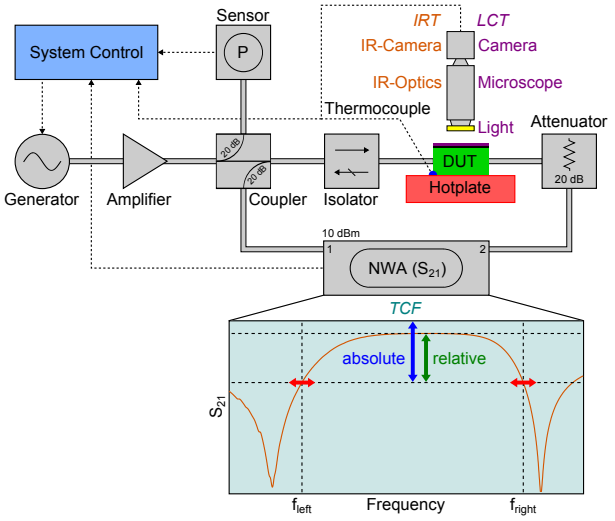

Fig. 3. Experimental setup for self-heating measurements by LCT, IRT, and TCF. Additionally, the evaluation procedure of the latter is depicted.

C. Thermography

There are numerous different approaches for nondestructive temperature measurements available, such as electrical and optical methods which may be physically contacting as well as noncontacting [3]. For conventional uncoated SAW devices only noncontacting methods can be used, while their acoustically passivated counterparts investigated in this work also allow the application of contacting measurement techniques. This is due to the negligible amplitude of the acoustic wave at the surface which is passivated with a thick TCF reducing SiO_2 layer. As we intend to measure the spatial distribution of the temperature, only techniques are considered which are capable of thermal mapping.

Liquid Crystal Thermography (LCT) is a popular temperature measurement technique in nondestructive testing of electronic devices and relies on Thermochromic Liquid Crystals (TLCs) which selectively reflect incident white light depending on their temperature [4]. The TLC molecules are helically structured with a periodicity in the order of the wavelength of visible light. Due to the temperature dependent pitch of the helix TLCs scatter incident white light selectively by wavelength, with the selectivity being a function of temperature. Thus, the apparent color of the observed region changes as its temperature changes.

Infrared Thermography (IRT) is probably the most common optical technique for measuring temperatures. It relies on the fact that all matter spontaneously radiates energy above absolute zero as a consequence of its temperature. With knowledge of the emissivity the temperature of a body can be determined by measuring its total emitted radiation.

III. Experimental Procedure

Previously, we already reported in detail on the complete experimental procedure including sample preparation, emissivity correction for IRT, and TLC calibration as well as post-processing for LCT [5, 6]. Thus, we only describe the measurement setup employed for the self-heating experiments reported here (Fig. 3). The RF generator is connected to the power amplifier which feeds the DUT via a directional coupler. A power sensor detects the applied power and a Network Analyzer (NWA) measures the transfer function of the Device Under Test (DUT) for TCF based temperature evaluations. Protection of the NWA and the power amplifier is ensured by an attenuator and an isolator. The signal path and its frequency-dependent power attenuation is calibrated for all load frequencies. In order to raise the ambient temperature closely below the TLC's active temperature range the DUT is placed on a hotplate, the temperature of which is measured by a thermocouple. A digital color camera captures the LCT color distribution on the illuminated DUT via a microscope while adjusting gain and exposure time automatically for each image. The IR camera (InfraTec ImageIR) records thermal maps of

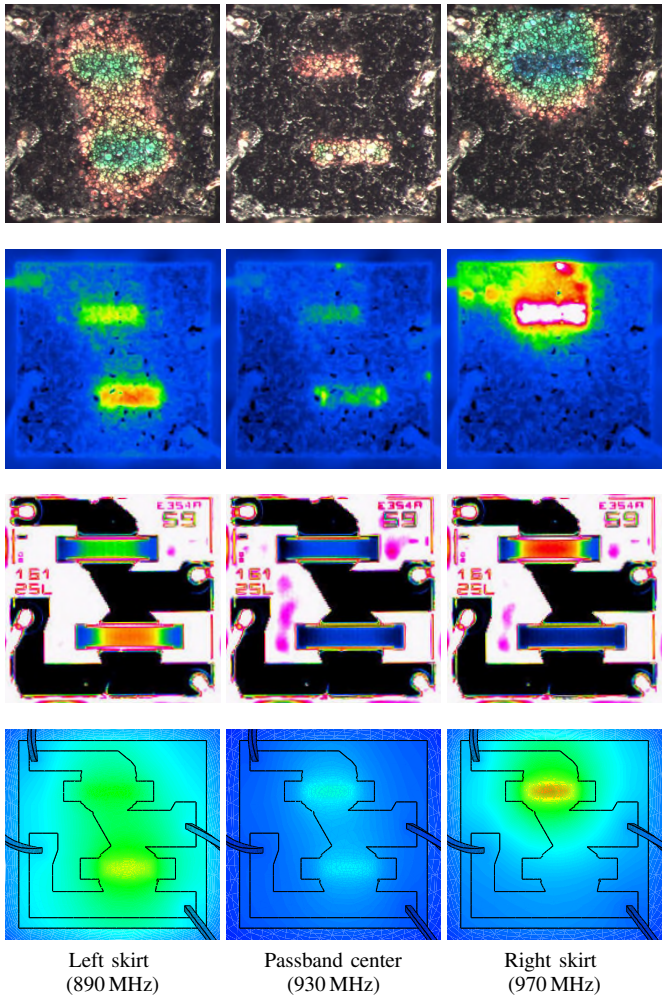

Fig. 4. Qualitative temperature distributions on a half-section ladder-type SAW filter with thick SiO_2 coating under load ($P = 25$ dBm): Measured by LCT (top panel), measured by IRT with (second panel) and without (third panel) black backing paint, and simulated using FEM (bottom panel). All are shown for three different load frequencies, at about the left skirt, at the passband center, and near to the right skirt of the filter.

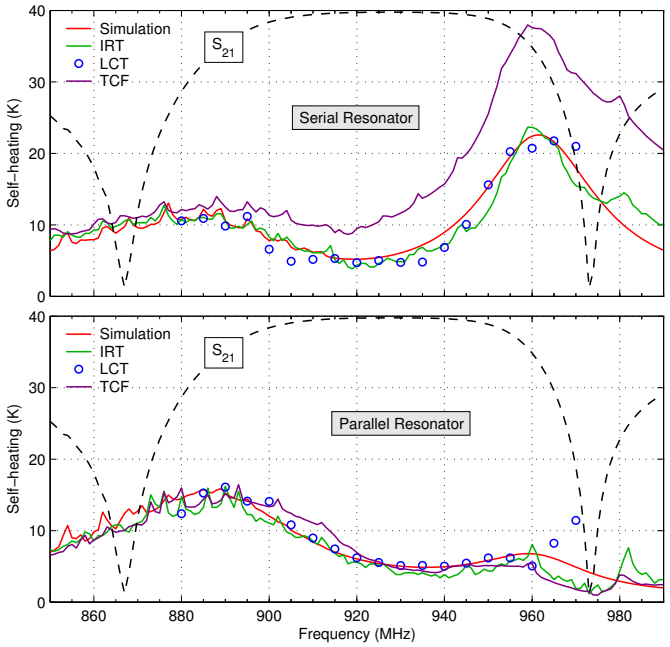

Fig. 5. Self-heating of both resonators as a function of load frequency at a load power of $P = 25\,\mathrm{dBm}$: Simulation compared with IRT, LCT, and TCF measurement results. The transfer function S_{21} of the filter is shown as a reference in arbitrary units.

the DUT taking into consideration its previously determined emissivity. The entire measurement setup is controlled by a LabVIEW program which sets load frequency and power at the RF generator and reads out the NWA, the power sensor, the thermocouple, and both cameras.

IV. Results and Discussion

Qualitative temperature distributions of the DUT under load are visualized in Fig. 4. The top panel illustrates raw LCT images at three different load frequencies, at the left skirt, at the passband center, and at the right skirt of the filter. Since these images are not post-processed and converted to temperature values, they reveal the actual TLC color distribution on the component's surface ranging from red to blue corresponding to approximately 60°C and 80°C, respectively [5, 6]. The second and third panel show the associated IRT measurements with and without black backing paint. According FEM simulation results are depicted in the bottom panel. The basis for the simulation of the temperature distribution are spatially resolved track and global pad losses shown in Fig. 2 resulting from simulated acoustic and electromagnetic energy fields. In this context, heat conduction and convection of the entire sample comprising chip, PCB, bond wires and epoxy adhesive are taken into account.

In Fig. 5 the measured self-heating of both resonators as determined by IRT, LCT, and TCF is analyzed quantitatively as a function of load frequency and compared with simulation results. While TCF based evaluations yield a scalar temperature increase, simulation and both thermographic measurement techniques result in thermal maps of the entire chip. In these cases, the self-heating is determined by evaluating the maximum temperature rise in each resonator. By means of the maximum occurring temperature value defined by the TLC calibration the heat transfer coefficient in simulation is adjusted to match the measurement.

Thereby, good agreement between results of both thermographic methods and simulation is observed. The small deviations between IRT and simulation results in terms of local temperature maxima measured by IRT at about 960 MHz and 980 MHz originate from spurious mode responses which are out of the simulation's scope. Nevertheless, big discrepancies occur between TCF based evaluation and the other results. This could be caused by the fact that temperatures determined that way are attributed homogeneously to the entire chip without taking local inhomogeneities into account. Furthermore, it is noticeable that deviations are especially observed at the serial resonator which is evaluated at its antiresonance. Anyhow, apart from temperature there could be other physical effects causing a frequency shift. Hence, at least for the serial resonator TCF based evaluation is an unsuitable tool to precisely ascertain the device temperature and should be substituted by thermographic techniques.

V. Conclusion

In this work, we investigated different schemes for thermal characterization of a half-section ladder-type SAW filter which is acoustically passivated with a thick SiO_2 layer. Unitarity violation quantifies the entire power loss in the device but is unfeasible regarding correlation to each resonator. The TCF characterizes thermally induced frequency shifts and has the potential to investigate the resonators' temperatures separately in first order. However, uncertainties arise using this indirect approach as soon as other effects causing a frequency shift play a role. Thermographic techniques such as IRT and LCT serve as direct measurement schemes eliminating inaccuracies inherent to TCF based evaluations and show good agreement with simulation results. Moreover, LCT and IRT provide spatially resolved temperature measurements of the component.

References

[1] T. Nishihara, H. Uchishiba, T. Matsuda, O. Ikata, and Y. Satoh, "Improvement in power durability of SAW filters," in *Proc. IEEE International Ultrasonics Symposium (IUS)*, 1995, pp. 383–388.

[2] K. Hashimoto, M. Kadota, T. Nakao, M. Ueda, M. Miura, H. Nakamura, H. Nakanishi, and K. Suzuki, "Recent development of temperature compensated SAW devices," in *Proc. IEEE International Ultrasonics Symposium (IUS)*, 2011, pp. 79–86.

[3] P. R. N. Childs, J. R. Greenwood, and C. A. Long, "Review of temperature measurement," *Review of Scientific Instruments*, vol. 71, pp. 2959–2978, 2000.

[4] C. R. Smith, D. R. Sabatino, and T. J. Praisner, "Temperature sensing with thermochromic liquid crystals," *Experiments in Fluids*, vol. 30, pp. 190–201, 2001.

[5] C. Huck, H. P. Zidek, T. Ebner, K. C. Wagner, and A. Wixforth, "Liquid crystal thermography on coated SAW devices," in *Proc. IEEE International Ultrasonics Symposium (IUS)*, 2012, pp. 2493–2496.

[6] C. Huck, H. P. Zidek, T. Ebner, K. C. Wagner, and A. Wixforth, "Liquid crystal and infrared thermography on coated SAW devices," in *Proc. European Microwave Conference (EuMC)*, 2013 [in press].